

Synchronization of Weighted Essentially Non-Oscillatory Methods

Ellen M. Taylor and M. Pino Martin*

*Department of Mechanical and Aerospace Engineering, Princeton University,
Princeton, NJ 08544, USA.*

Received 17 June 2007; Accepted (in revised version) 6 November 2007

Communicated by Weinan E

Available online 27 February 2008

Abstract. Weighted essentially non-oscillatory (WENO) methods have been developed to simultaneously provide robust shock-capturing in compressible fluid flow and avoid excessive damping of fine-scale flow features such as turbulence. Under certain conditions in compressible turbulence, however, numerical dissipation remains unacceptably high even after optimization of the linear component that dominates in smooth regions. Of the *nonlinear* error that remains, we demonstrate that a large fraction is generated by a “synchronization deficiency” that interferes with the expression of theoretically predicted numerical performance characteristics when the WENO adaptation mechanism is engaged. This deficiency is illustrated numerically in simulations of a linearly advected sinusoidal wave and the Shu-Osher problem [J. Comput. Phys., 83 (1989), pp. 32-78]. It is shown that attempting to correct this deficiency through forcible synchronization results in violation of conservation. We conclude that, for the given choice of candidate stencils, the synchronization deficiency cannot be adequately resolved under the current WENO smoothness measurement technique.

AMS subject classifications: 76F65

Key words: Direct numerical simulation, large eddy simulation, compressible turbulence, shock capturing.

1 Introduction

The detailed simulation of compressible turbulence requires numerical methods that simultaneously avoid excessive damping of spatial features over a large range of length scales and prevent spurious oscillations near shocks and shocklets (small transient shocks) through robust shock-capturing. Numerical schemes that were developed to satisfy these

*Corresponding author. *Email addresses:* emtaylor@princeton.edu (E. M. Taylor), pmartin@princeton.edu (M. P. Martin)

constraints include, among others, weighted essentially non-oscillatory (WENO) methods [2]. WENO schemes compute numerical fluxes using several different candidate stencils and form a final flux approximation by summing weighted contributions from each stencil. Thus they are nonlinear. Smoothness measurements cause stencils that span large flow field gradients to be assigned small relative weights so that a nearly discontinuous shock would provide a weight of almost zero to any stencil containing it. In smooth regions, the relative values of the weights are designed to be optimal by some gauge such as maximum order of accuracy or maximum bandwidth-resolving efficiency.

Jiang and Shu [3] cast the WENO methodology into finite-difference form and provide an efficient implementation of robust and high-order-accurate WENO schemes. Unfortunately, these schemes often generate excessive numerical dissipation for detailed simulations of turbulence, especially for large-eddy simulations (LES) [4]. WENO dissipation arises from two distinct sources: (i) the optimal stencil, which by itself describes a linear scheme, and (ii) the adaptation mechanism, which drives the final numerical stencil away from the optimal one. Bandwidth optimization can reduce the dissipation of the optimal stencil [5–7]; and Martín et al. [7] demonstrate that such a bandwidth-optimized symmetric WENO method indeed reduces numerical dissipation and provides accurate results for direct numerical simulations (DNS) of isotropic turbulence and turbulent boundary layers.

Nonetheless, engaging the nonlinear WENO adaptation mechanism still causes significant local dissipation that can negatively affect global flow properties. Though higher resolution compensates for this, in some cases adequately increasing the number of grid points is not feasible. There are two primary sources of nonlinear error: (i) the smoothness measurement that governs the application of WENO stencil adaptation and (ii) the numerical properties of individual candidate stencils that govern numerical accuracy when adaptation engages. Wang and Chen [8] have examined both sources for upwind-biased WENO methods in linearized problems; Ponziani et al. [9] have examined the second source for symmetric WENO methods in linear and nonlinear problems, including isotropic turbulence; and Henrick et al. [10] have examined the first source for upwind-biased WENO methods in linear and nonlinear problems. Additionally, Taylor et al. [11] have examined the first source for symmetric WENO methods in linear and nonlinear problems, including isotropic turbulence, and have introduced a linearly and nonlinearly optimized WENO method that allows accurate DNS of compressible turbulence with significantly reduced grid sizes [11, 12].

The purpose of this paper is to demonstrate that there exists a WENO “synchronization deficiency” that interferes with the expression of theoretically predicted candidate stencil properties and as a result generates excessive numerical dissipation through the second nonlinear error pathway described above. We furthermore attempt to correct this deficiency by exploring the possibility of forcible synchronization, and in the process we enumerate the several serious theoretical and practical obstacles that currently prevent an implementation of this approach that is both robust and broadly applicable. Section 2 briefly describes the WENO methodology. In Section 3, we introduce the mathematical

and theoretical basis of the synchronization deficiency and present numerical evidence of its consequences through simulations of a linearly advected sinusoidal wave and a one-dimensional inviscid shock/entropy-wave interaction that we refer to as the Shu-Osher problem. Section 3.3 then discusses the aforementioned obstacles to implementing forcible synchronization as a corrective measure. Finally, conclusions are drawn in Section 4.

2 WENO methodology

We describe the symmetric WENO methodology [5–7] in the context of the one-dimensional advection equation,

$$\frac{\partial u}{\partial t} + \frac{\partial}{\partial x} f(u) = 0. \quad (2.1)$$

This model equation represents the decoupled forms of equations belonging to any system of hyperbolic conservation laws after a transformation from physical into characteristic space. If the spatial domain is discretized such that $x_i = i\Delta$, in which Δ is the grid spacing, and $u_i = u(x_i)$, Eq. (2.1) may be cast into the semi-discretized form

$$\frac{du_i}{dt} = -\frac{1}{\Delta} (\hat{f}_{i+\frac{1}{2}} - \hat{f}_{i-\frac{1}{2}}) \quad (2.2)$$

in which $\hat{f}_{i+1/2}$ is a numerical approximation of $f(u(x_{i+1/2}))$. Once the right-hand side of this expression has been evaluated, numerical techniques for solving ordinary differential equations, such as Runge-Kutta methods, may be employed to advance the solution in time. In order to ensure stability, procedures that approximate $f(u)$ split it into $f^+(u)$, which has a strictly non-negative derivative, and $f^-(u)$, which has a strictly non-positive one.

WENO schemes compute $\hat{f}_{i+1/2}^+$ through reconstructed interpolating polynomials on a number of candidate stencils each containing r grid points. In the symmetric WENO method, there are $(r+1)$ stencils in total. The one fully upwinded stencil ranges from $(i-r+1)$ to i , the one fully downwinded stencil ranges from $(i+1)$ to $(i+r)$, and the other stencils fall in between these two extremes. Fig. 1 provides a schematic of this arrangement for $r=3$. Throughout this paper, we will abbreviate any WENO implementation in which the candidate stencils contain r points as “WENO- r .”

If the flux approximation on stencil k , which contains r grid points, is designated as q_k^r and the weight assigned to that stencil is ω_k , the final numerical approximation becomes

$$\hat{f}_{i+\frac{1}{2}}^+ = \sum_{k=0}^r \omega_k q_k^r. \quad (2.3)$$

Specifically, q_k^r emerge from reconstructed polynomial interpolants of maximal order r and are defined as

$$q_k^r \Big|_{i+\frac{1}{2}} = \sum_{l=0}^{r-1} a_{kl}^r f(u_{i-r+k+l+1}) \quad (2.4)$$

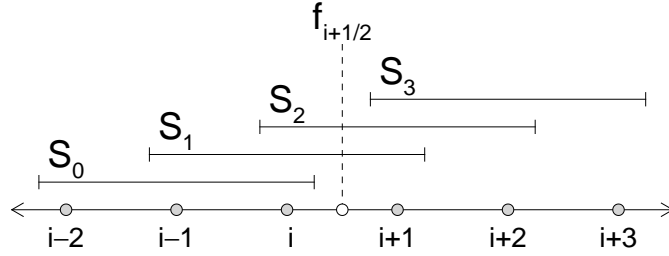


Figure 1: Symmetric WENO candidate stencils for approximating the numerical flux $\hat{f}_{i+1/2}^+$ when the number of points per candidate stencil is $r=3$.

in which a_{kl}^r are tabulated coefficients; and ω_k are normalized forms of weights Ω_k defined as

$$\Omega_k = \frac{C_k^r}{(\varepsilon + IS_k)^p} \quad (2.5)$$

in which ε prevents division by zero, IS_k is a smoothness measurement that becomes large when discontinuities are present within stencil k , and p may be varied to increase or decrease WENO adaptation sensitivity. $p=1$ typically provides sufficient adaptation with minimal dissipation. In completely smooth regions, each stencil is equally desirable, and ω_k revert to the optimal weights C_k .

The corresponding stencil diagram for $\hat{f}_{i+1/2}^-$ is simply a mirror image of Fig. 1. Because the total number of data points available to the symmetric WENO algorithm is $2r$, its maximum order of accuracy is also $2r$; however, the optimal stencils employed in the current work are bandwidth-optimized [5–7] such that only r th-order accuracy can be guaranteed. The bandwidth-optimization process also introduces a small amount of artificial dissipation to an otherwise neutrally stable optimal stencil to enhance its stability. In practice, the weight of the fully downwinded stencil ω_r is artificially constrained to be no greater than the least of the others so that other adverse stability effects are avoided.

The continuity of the WENO weighting process allows the performance characteristics of the final numerical stencil to theoretically fall anywhere between those of the least favorable candidate stencil and those of the optimal stencil. In order to gauge this variation quantitatively but efficiently in a flow field, Weirs [6] proposed a combination of the adaptive stencil weights called the nonlinearity index (NI). It is essentially a measure of the degree of departure from the optimal stencil and is defined as

$$NI = \left(\sum_{k=0}^r \left[1 - \frac{(r+1)(\Omega_k/C_k)}{\sum_{l=0}^r (\Omega_l/C_l)} \right]^2 \right)^{\frac{1}{2}}. \quad (2.6)$$

This definition forces NI to always be non-negative, and only the optimal stencil can provide a value of zero. It reaches its theoretical maximum, which is $\sqrt{r(r+1)}$, when any one candidate stencil is chosen exclusively. We will often report NI in terms of NI' , its value normalized by this maximum.

3 Synchronization deficiency

3.1 Theory

In theory, the numerical performance characteristics (e.g. bandwidth-resolving capabilities) of the least favorable WENO candidate stencil dictate definitive lower bounds on the performance characteristics of any possible final weighted numerical stencil. If the flux approximation $\hat{f}_{i+1/2}$, calculated according to the previous section, were to encompass the entirety of the flux information required to approximate a spatial derivative, then this would be true in practice as well. Of course, in addition to $\hat{f}_{i+1/2}$, Eq. (2.2) demands $\hat{f}_{i-1/2}$, which is rarely explicitly acknowledged because its calculation consists merely of shifting an index. Its presence, however, significantly complicates the question of performance characteristics, as has been briefly mentioned, but not further investigated, by Henrick et al. [10].

Let us fully expand Eq. (2.2), the left-hand side of which depends on a fixed combination of $\hat{f}_{i+1/2}$ and $\hat{f}_{i-1/2}$. According to Eqs. (2.3) and (2.4),

$$\hat{f}_{i+\frac{1}{2}} = \sum_{k=0}^r \omega_k \sum_{l=0}^{r-1} a_{kl}^r f_{i-r+k+l+1} \quad (3.1a)$$

$$\hat{f}_{i-\frac{1}{2}} = \sum_{k=0}^r \omega_k \sum_{l=0}^{r-1} a_{kl}^r f_{i-r+k+l} \quad (3.1b)$$

and so

$$\begin{aligned} \frac{du_i}{dt} &= -\frac{1}{\Delta} \left(\hat{f}_{i+\frac{1}{2}} - \hat{f}_{i-\frac{1}{2}} \right) \\ &= -\frac{1}{\Delta} \sum_{k=0}^r \omega_k \left[a_{k,r-1}^r f_{i+k} - a_{k,0}^r f_{i-r+k} + \sum_{l=1}^{r-1} (a_{k,l-1}^r - a_{kl}^r) f_{i-r+k+l} \right] \\ &= -\frac{1}{\Delta} \sum_{k=0}^r \omega_k \sum_{l=0}^r b_{kl}^r f_{i-r+k+l} \end{aligned} \quad (3.2)$$

in which coefficients can be equated to yield

$$b_{kl}^r = \begin{cases} -a_{k,0}^r, & l=0, \\ a_{k,l-1}^r - a_{kl}^r, & 0 < l < r, \\ a_{k,r-1}^r, & l=r. \end{cases} \quad (3.3)$$

The coefficients b_{kl}^r , rather than a_{kl}^r , are the relevant parameters for determining and optimizing the properties of the k th candidate stencil. Since b_{kl}^r are independent of the adaptive stencil weights ω_k , the performance characteristics of individual candidates appear to be guaranteed regardless of local WENO adaptation behavior. Unfortunately, this appealing argument is contingent upon the implicit assumption in Eq. (3.1) that ω_k are equal for $\hat{f}_{i+1/2}$ and $\hat{f}_{i-1/2}$.

The smoothness measurement IS_k depends entirely on the flux information available within the k th candidate stencil, which spans different points for $\hat{f}_{i+1/2}$ and $\hat{f}_{i-1/2}$. Because the collections of data values on the two versions of the stencil will in general be unequal, the associated stencil weights ω_k must be assumed to vary. If we define ω_k^\pm to mean the ω_k that belong to $\hat{f}_{i\pm 1/2}$, Eq. (3.1) becomes

$$\hat{f}_{i+\frac{1}{2}} = \sum_{k=0}^r \omega_k^+ \sum_{l=0}^{r-1} a_{kl}^r f_{i-r+k+l+1} \quad (3.4a)$$

$$\hat{f}_{i-\frac{1}{2}} = \sum_{k=0}^r \omega_k^- \sum_{l=0}^{r-1} a_{kl}^r f_{i-r+k+l} \quad (3.4b)$$

and in turn Eq. (3.2) becomes

$$\begin{aligned} \frac{du_i}{dt} &= -\frac{1}{\Delta} \left(\hat{f}_{i+\frac{1}{2}} - \hat{f}_{i-\frac{1}{2}} \right) \\ &= -\frac{1}{\Delta} \sum_{k=0}^r \omega_k^+ \left[a_{k,r-1}^r f_{i+k} - \frac{\omega_k^-}{\omega_k^+} a_{k,0}^r f_{i-r+k} + \sum_{l=1}^{r-1} \left(a_{k,l-1}^r - \frac{\omega_k^-}{\omega_k^+} a_{kl}^r \right) f_{i-r+k+l} \right] \\ &= -\frac{1}{\Delta} \sum_{k=0}^r \omega_k^+ \sum_{l=0}^r \widetilde{b}_{kl}^r f_{i-r+k+l} \end{aligned} \quad (3.5)$$

in which coefficients can be equated to yield

$$\widetilde{b}_{kl}^r = \begin{cases} -\frac{\omega_k^-}{\omega_k^+} a_{k,0}^r, & l=0, \\ a_{k,l-1}^r - \frac{\omega_k^-}{\omega_k^+} a_{kl}^r, & 0 < l < r, \\ a_{k,r-1}^r, & l=r. \end{cases} \quad (3.6)$$

The relevant parameters for determining and optimizing the properties of the k th candidate stencil are now the new coefficients \widetilde{b}_{kl}^r . These, unlike the old b_{kl}^r , do depend on the adaptive quantities ω_k^\pm ; and, since a_{kl}^r are fixed, $\widetilde{b}_{kl}^r = b_{kl}^r$ if and only if $\omega_k^- = \omega_k^+$. Note that equality necessarily holds when $\hat{f}_{i\pm 1/2}$ both employ the optimal stencil weights C_k^r . However, in regions in which WENO adaptation has engaged, either necessarily or unnecessarily, inequality can force the actual individual stencil characteristics to diverge from the expected theoretical properties described by b_{kl}^r .

The theoretical error characteristics of a finite-difference scheme are often quantitatively presented in the form of a modified wavenumber plot, which illustrates theoretical bandwidth properties. Consider a linearly advected pure harmonic function of the form

$$f(x) = e^{ikx} = e^{i\kappa x/\Delta} \quad (3.7)$$

in which x is position, Δ is grid spacing, and k and κ are dimensional and nondimensional wavenumbers, respectively. The finite-difference approximation to its spatial derivative

is equivalent to the analytic derivative of a similarly defined function with the modified wavenumber

$$\kappa'(\kappa) = -i \sum_n c_n e^{in\kappa} \quad (3.8)$$

in which c_n are constant nondimensional coefficients unique to a particular scheme. The real and imaginary parts of κ' describe phase and amplitude characteristics, respectively, and a numerical method that fully resolved all wavenumbers would produce $\kappa' = \kappa$ for $0 \leq \kappa \leq \pi$. In the present case of symmetric WENO methods,

$$c_n = \begin{cases} -\omega_0^- a_{0,0}^r, & n = -r, \\ \sum_{m=0}^{r+n-1} \omega_m^+ a_{m,r+n-m-1}^r - \sum_{m=0}^{r+n} \omega_m^- a_{m,r+n-m}^r, & -r < n < 0, \\ \sum_{m=0}^{r-1} \omega_m^+ a_{m,r-m-1}^r - \sum_{m=1}^r \omega_m^- a_{m,r-m}^r, & n = 0, \\ \sum_{m=n}^r \omega_m^+ a_{m,r+n-m-1}^r - \sum_{m=n+1}^r \omega_m^- a_{m,r+n-m}^r, & 0 < n < r, \\ \omega_r^+ a_{r,r-1}^r, & n = r. \end{cases} \quad (3.9)$$

In Fig. 2, we plot the modified wavenumber of the linearly optimized WENO-3 scheme for an illustrative possible scenario in which the stencil weights are such that, for the calculation $\hat{f}_{i-1/2}$ ("left-hand" calculation), the first *three* stencils are equally utilized and the last one discarded, and for the calculation of $\hat{f}_{i+1/2}$ ("right-hand" calculation), the first *two* stencils are equally utilized and the last two discarded. Fig. 1 provides a useful graphical reference for visualizing this scenario. Since the left-hand arrangement incorporates more grid points and is more centrally situated relative to the point of interest x_i , we would expect its numerical characteristics to be more favorable than those of the right-hand arrangement. Indeed, Fig. 2(a) confirms that if both calculations were forced to use the left-hand arrangement ("synchronized left") rather than the right-hand one ("synchronized right"), κ' would more closely approximate κ . Though at first glance the unsynchronized arrangement might seem as if it should lead to bandwidth properties that split the difference, the modified wavenumber plot reveals that its amplitude characteristics are only slightly better than those of the worst component and that its phase characteristics are actually significantly poorer. Deviations of phase characteristics from the exact relationship $\kappa'(\kappa) = \kappa$ can be seen more clearly in Fig. 2(b), which plots the phase error $\varepsilon = \kappa' / \kappa - 1$.

3.2 Numerical evidence

Though the WENO synchronization deficiency is certainly valid from a mathematical standpoint, and even though it can under certain circumstances significantly degrade theoretical bandwidth properties, its cumulative effects on actual numerical simulations may still turn out to be relatively small. We investigate this possibility by implementing

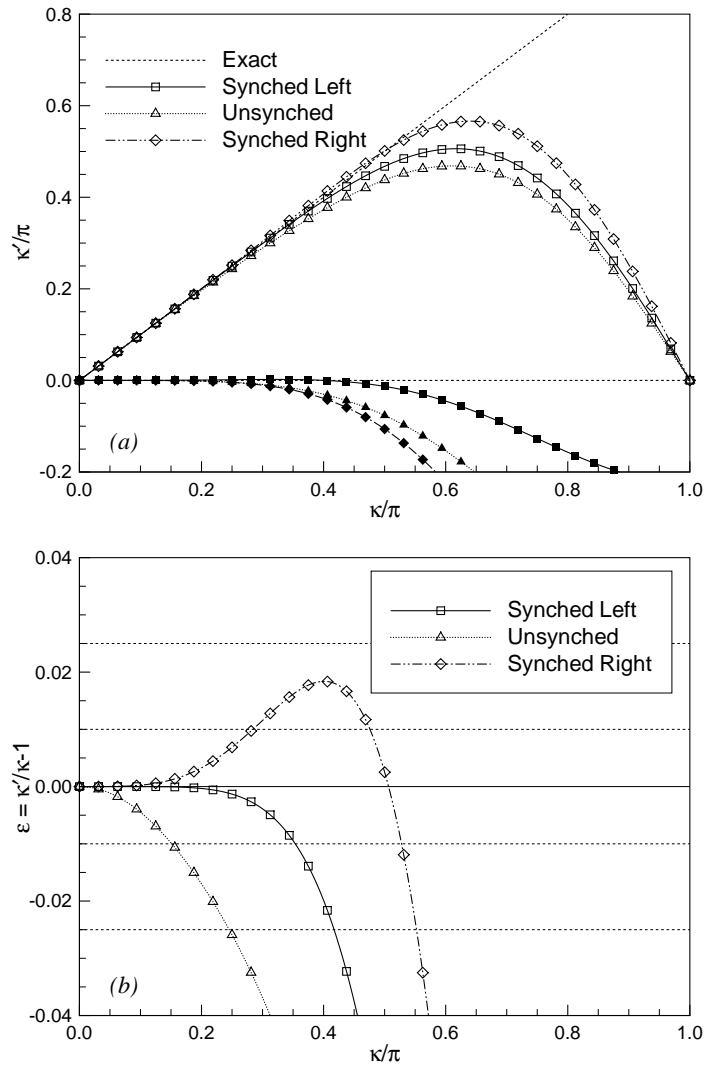


Figure 2: Bandwidth properties of the WENO-3 scheme when the “left-hand” calculation utilizes only the first three candidate stencils equally and the “right-hand” calculation utilizes only the first two equally. Open and filled symbols indicate phase and amplitude characteristics, respectively. (a) Modified wavenumber. (b) Modified wavenumber error.

a naive forcibly synchronized WENO (SWENO) method for the one-dimensional advection equation of Eq. (2.1). After obtaining the normalized stencil weights ω_k according to Section 2, we set

$$\langle \Omega_k \rangle = \frac{1}{2} (\omega_k^+ + \omega_k^-) \quad (3.10)$$

and then normalize $\langle \Omega_k \rangle$ to form the synchronized stencil weights $\langle \omega_k \rangle$ that apply to calculations of both $\hat{f}_{i+1/2}$ and $\hat{f}_{i-1/2}$.

The effects of synchronizing the linearly optimized WENO-4 scheme in this man-

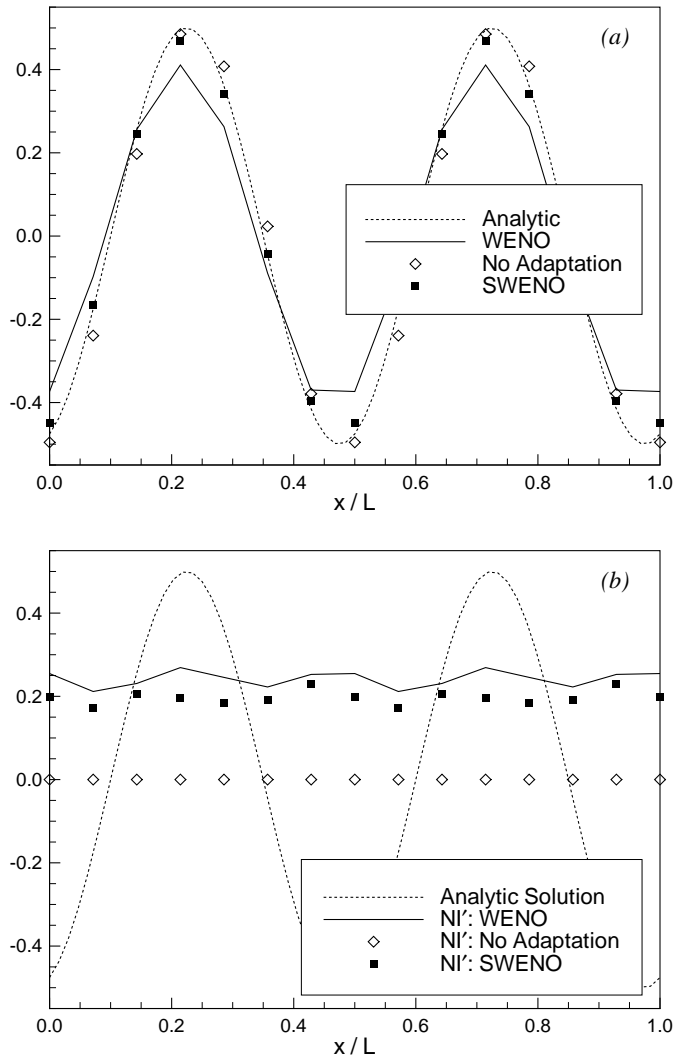


Figure 3: Linearly advected sinusoidal wave with seven points per wavelength as computed by the WENO-4 scheme, with and without adaptation, and the forcibly synchronized WENO-4 (SWENO-4) scheme after twenty wavelength-times. (a) Numerical and analytic solutions. (b) Nonlinearity index.

ner are presented in Fig. 3, which depicts a linearly advected sinusoidal wave with seven points per wavelength after time integration via a third-order-accurate Runge-Kutta scheme for twenty wavelength-times. For reference we include results from the baseline (unsynchronized) WENO-4 scheme both with and without stencil adaptation permitted. The solution profiles of Fig. 3(a) show that, while the fully adapting WENO-4 scheme causes notable dissipation, the SWENO-4 scheme maintains the proper wave shape nearly as faithfully as when adaptation is completely prohibited and the optimal stencil uniformly employed. In Fig. 3(b), we plot the nonlinearity index NI' for each of

these schemes to demonstrate that the improvement offered by the SWENO method is not due simply to closer conformance to the optimal stencil. The decrease in overall NI' from the adaptation-permitted WENO-4 scheme to the adaptation-prohibited scheme far exceeds the decrease from the former to the SWENO-4 scheme, yet the SWENO-4 flow solution is almost equivalent to the adaptation-prohibited solution.

Attempting to extend the forcible synchronization technique of Eq. (3.10) to non-smooth data exposes several serious problems concerning its application to immediate neighborhoods of strong discontinuities, but we will defer the full discussion of these until the following section. For now, we present additional numerical evidence with the understanding that synchronization is selectively suspended near discontinuities in a somewhat ad-hoc and overly conservative manner not intended for general use.

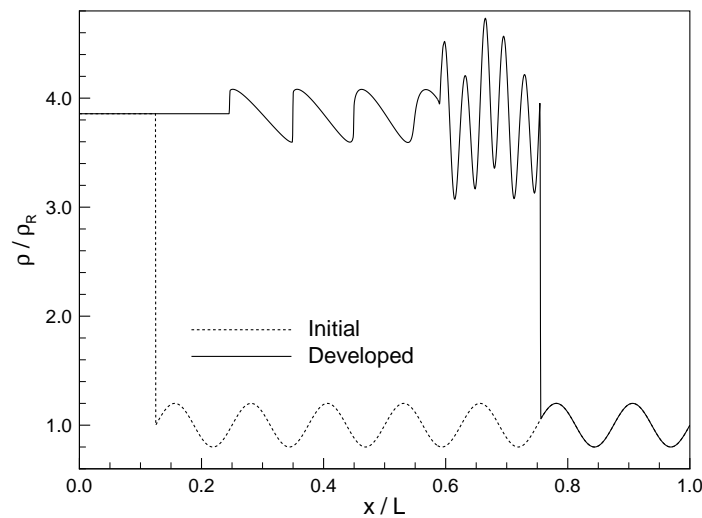


Figure 4: Initial and developed density profiles of the Shu-Osher problem as computed on 2048 grid points by the WENO-4 scheme.

The Shu-Osher problem [1] places smooth density fluctuations upstream of a moving shock front to probe the ability of a shock-capturing method to resolve discontinuities embedded within pseudoturbulence without damaging fine structures. In our simulations, the conditions at the right boundary are atmospheric with zero velocity, and the conditions at the left boundary are such that the shock between the two states has a relative incoming Mach number of three. Sinusoidal density fluctuations are imposed upstream of this shock (in a frame of reference moving with the shock wave) with wavelength $\lambda = \frac{1}{8}L$ and excursions of $\pm 0.2\rho_R$, in which the subscript R indicates the right boundary. Initially, the shock is positioned at $x/L = \lambda$, and we evolve simulations in time via a third-order-accurate Runge-Kutta scheme until $t = 0.21L/a_R$. For reference, Fig. 4 displays converged density profiles for the initial and developed states as computed by the WENO-4 scheme on an excessively fine grid of 2048 points. Upon termination, an undisturbed portion of the original fluctuation field lies upstream of the main shock, im-

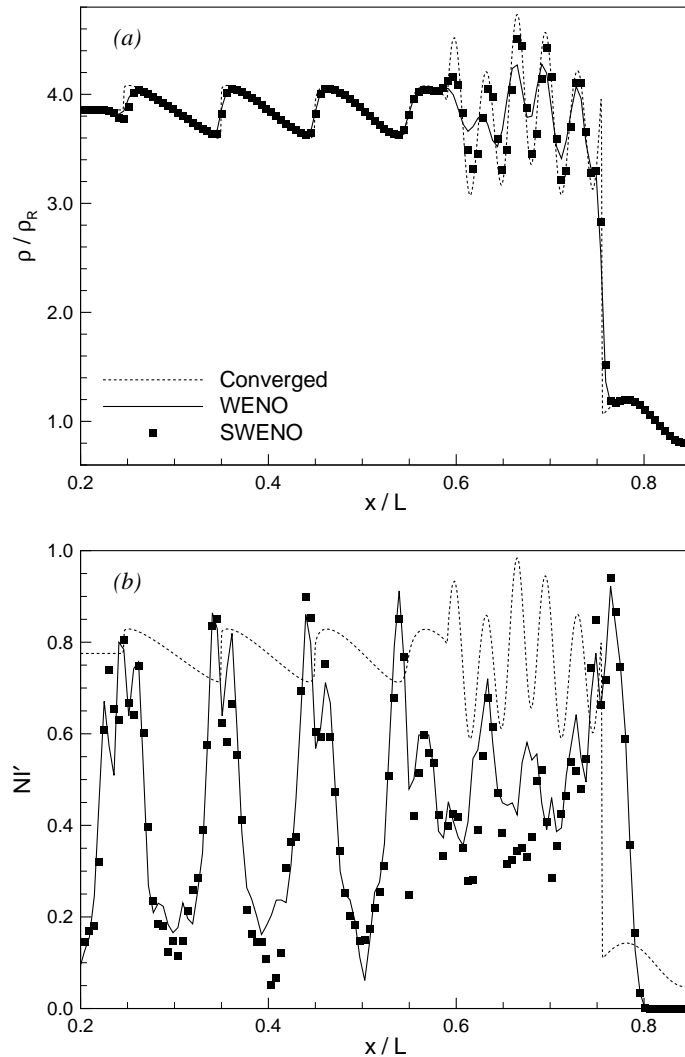


Figure 5: Flow profiles of the Shu-Osher problem as computed on 192 grid points by WENO-3 and forcibly synchronized WENO-3 (SWENO-3) schemes. (a) Density. (b) Nonlinearity index.

mediately downstream is a region of physically correct high-frequency fluctuations, and further downstream is a region of low-frequency fluctuations with interspersed shocklets.

In Fig. 5, we examine the effects of selectively suspended forcible synchronization on solutions to the Shu-Osher problem as computed by the linearly optimized WENO-3 scheme on 192 grid points. Fig. 5(a) shows that, at this resolution, the density profile of the baseline unsynchronized WENO scheme is sufficiently accurate everywhere except within the high-frequency region, where excessive numerical dissipation severely damages its accuracy. The SWENO scheme, on the other hand, captures these fluctuations

significantly more faithfully, indicating that in this case the synchronization deficiency accounts for a large fraction of the excessive dissipation. Corresponding profiles of non-linearity index NI' are presented in Fig. 5(b), and their approximate equivalence between the WENO and SWENO schemes, especially near the edges of the high-frequency region, indicates that, as we observed in the previous case of the linearly advected sinusoidal wave, the benefits of forcible synchronization cannot be attributed simply to serendipitously closer conformance to the optimal stencil. A similar analysis of synchronized versus unsynchronized WENO-4 schemes yields results that are materially identical to these that were just presented for the WENO-3 schemes.

These exercises prove that the synchronization deficiency is not merely a mathematical curiosity; its consequences unquestionably contaminate the results of numerical simulations.

3.3 Obstacles to correction

As we noted previously, attempting to extend the forcible synchronization technique of Eq. (3.10) to non-smooth data exposes several serious problems concerning its application to immediate neighborhoods of strong discontinuities.

First, consider a linearly advected perfect shock located somewhere between points x_{i-1} and x_i as sketched for $r=3$ in Fig. 6. Without explicitly calculating the smoothness measurements IS_k and resulting weights ω_k , we can still qualitatively determine that a candidate stencil receives small weight if it crosses the discontinuity and large weight otherwise. Also, recall that the fully downwinded stencil is never allowed to hold more weight than the least-weighted of the others. According to these principles, the bold stencils in the lower portion of Fig. 6 are those independently favored for calculating $\hat{f}_{i\pm 1/2}$, and the two resulting stencil arrangements are clearly mutually exclusive. If ω_k^\pm are to be forcibly synchronized, some form of compromise is necessary; and any form of compromise under these circumstances will undermine the WENO shock-capturing mechanism.

Secondly, the form of the spatial derivative in Eq. (2.2) is not simply a matter of notational convenience. Across a shock located somewhere between points x_j and x_{j+1} , the flux leaving cell $i=j$ to the right ($\hat{f}_{i+1/2}=\hat{f}_{j+1/2}$) must precisely equal the flux entering cell $i=j+1$ from the left ($\hat{f}_{i-1/2}=\hat{f}_{j+1/2}$); otherwise, propagation of the shock front proceeds incorrectly. For the traditional WENO methodology, this proper flux behavior is guaranteed by the form of Eq. (2.2), coupled with the understanding that only $\hat{f}_{i+1/2}$ is explicitly computed at each grid point. Forcible synchronization, however, demands full and separate calculations of both $\hat{f}_{i\pm 1/2}$ in a manner that relies on local violation of the flux-conservation principle to effect any enhancement in bandwidth-resolving efficiency. That said, synchronization is not automatically a moribund concept because as the point of interest x_i moves away from the shock, the strictly conservative structure may be greatly relaxed, permitting finite-difference constructions that violate it, such as central Padé schemes [13], to be employed without consequence in smooth flow regions.

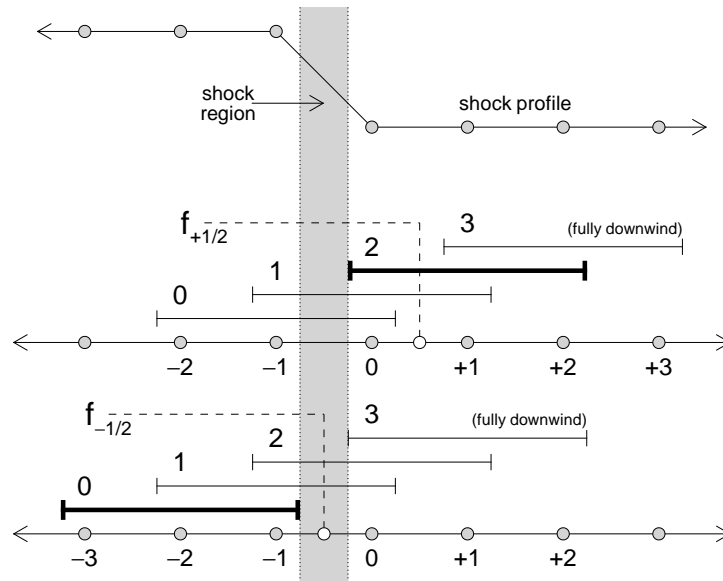


Figure 6: Symmetric WENO candidate stencils for approximating the dual numerical fluxes $\hat{f}_{i\pm 1/2}^+$ when the number of points per candidate stencil is $r=3$ and a perfect shock is located somewhere between points x_{i-1} and x_i . Bold stencils are strongly weighted.

Thus, in order to preserve the robust shock-capturing capability of unsynchronized WENO methods, we are required by two distinct theoretical considerations to selectively suspend synchronization in the immediate vicinity (i.e. within approximately one grid spacing) of strong discontinuities. Though in theory significant improvement of WENO dissipation performance is still possible under this constraint alone, as demonstrated by the Shu-Osher problem exercise in the previous section, there remains an additional consideration that is practical in nature.

The final and most intractable obstacle to forcible synchronization, or more precisely the suspension of synchronization, is that the WENO smoothness measurement technique, as currently formulated, cannot be trusted to distinguish with sufficient fidelity the non-smooth regions in which precise flux conservation is necessary versus those in which it is not. As an illustration, in Fig. 7 we plot the profiles of WENO-3 and WENO-4 nonlinearity index NI' that arise from a linearly advected shock wave with a numerical width between three and four grid spacings, which is typical of a well-captured shock. Immediately downstream and upstream of the shock front, high NI' indicates a sufficient impediment to inappropriate synchronization, but within the shock front, where strict flux conservation is paramount, NI' drops by almost half due to the illusion of smoothness imparted by numerical smearing. For the purpose of maintaining stability, such adaptation behavior is perfectly acceptable; it is disastrous, however, for the purpose of identifying contiguous shock regions in need of a conservative flux-differencing structure.

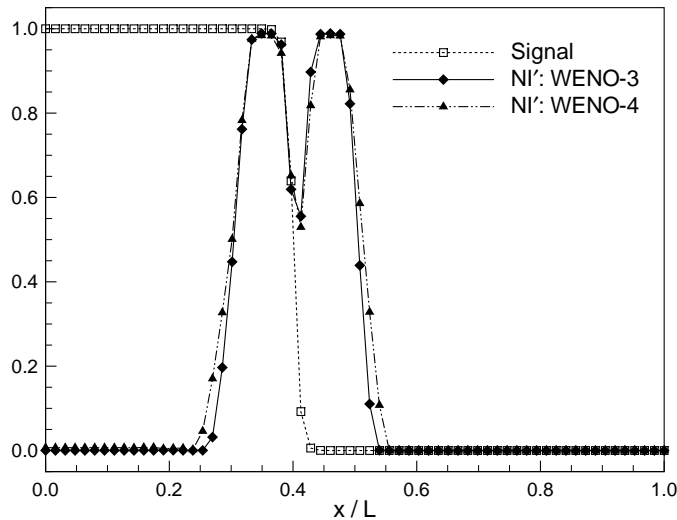


Figure 7: Profiles of WENO-3 and WENO-4 nonlinearity index NI' across a linearly advected shock wave with a numerical width between three and four grid spacings.

4 Conclusions

When adaptation draws the final numerical stencil away from the optimal stencil, WENO methods exhibit a synchronization deficiency between left- and right-hand flux calculations that interferes with the expression of theoretically predicted numerical performance characteristics. For an illustrative hypothetical stencil arrangement scenario, the modified wavenumber curve of the unsynchronized combination reveals substantially poorer theoretical bandwidth-resolving efficiency than even the least favorable synchronized combination. Furthermore, in linear advection simulations of smooth oscillations and also Euler simulations of the Shu-Osher problem, forcible synchronization, of an admittedly makeshift nature, significantly enhances numerical accuracy in practice as well. Based on these findings, we expect the synchronization deficiency to account for a large fraction of excessive dissipation in general compressible turbulent flows.

Forcible synchronization cannot be applied in the immediate vicinity (i.e. within approximately one grid spacing) of a discontinuity because to do so would undermine the robust shock-capturing capability of the WENO methodology. This constraint is dictated by theoretical considerations and is inviolable, but a discontinuity located toward the edges of the optimal stencil, triggering necessary but overly dissipative adaptation, can be deemed outside the immediate vicinity and would therefore theoretically permit the numerical performance benefits of synchronization to be realized locally. Unfortunately, the existing WENO smoothness measurement technique poorly distinguishes between non-smooth regions that require a strictly conservative flux-differencing structure, which is broken by synchronization, and those that do not. Thus, in order to guarantee

proper shock propagation, implementations of forcible synchronization must either be exquisitely tailored for specific flow configurations and conditions or excessively conservative such that synchronization benefits become unacceptably diluted.

Because the demonstrated degradation in bandwidth properties imparted by the WENO synchronization deficiency will almost certainly overwhelm any opposing enhancement offered by small changes to the individual candidate stencil coefficients, we recommend against attempting to improve WENO performance through bandwidth-optimization of these coefficients, as was conducted by Wang and Chen [8] and Ponziani et al. [9]. Any gains produced by this approach should be miniscule and effected primarily through the increased bandwidth-resolving efficiency this may allow to the *linear* optimal stencil. The WENO smoothness measurement technique, on the other hand, has become an even more attractive investigative target than before. If the smoothness measurement could be made to more faithfully identify contiguous shock-spanning regions, then in addition to any direct advantages conferred upon unsynchronized WENO schemes, the opportunities for robust forcible synchronization could perhaps be expanded to the point of true usefulness.

Acknowledgments

This work was sponsored by the National Science Foundation under Grant CTS-0238390. Computational resources were provided by the CRoCCo Laboratory at Princeton University.

References

- [1] C. W. Shu and S. Osher, Efficient implementation of essentially non-oscillatory shock-capturing schemes, II, *J. Comput. Phys.*, 83(1) (1989), 32-78.
- [2] X. D. Liu, S. Osher and T. Chan, Weighted essentially non-oscillatory schemes, *J. Comput. Phys.*, 115(1) (1994), 200-212.
- [3] G. S. Jiang and C. W. Shu, Efficient implementation of weighted ENO schemes, *J. Comput. Phys.*, 126(1) (1996), 202-228.
- [4] E. Garnier, M. Mossi, P. Sagaut, P. Comte and M. Deville, On the use of shock-capturing schemes for large-eddy simulations, *J. Comput. Phys.*, 153(1) (1999), 273-311.
- [5] V. G. Weirs and G. V. Candler, Optimization of weighted ENO schemes for DNS of compressible turbulence, Paper 1997-1940, American Institute of Aeronautics and Astronautics, 1997.
- [6] V. G. Weirs, A numerical method for the direct simulation of compressible turbulence, PhD thesis, University of Minnesota, December 1998.
- [7] M. P. Martín, E. M. Taylor, M. Wu and V. G. Weirs, A bandwidth-optimized WENO scheme for the effective direct numerical simulation of compressible turbulence, *J. Comput. Phys.*, 220(1) (2006), 270-289.
- [8] Z. J. Wang and R. F. Chen, Optimized weighted essentially nonoscillatory schemes for linear waves with discontinuity, *J. Comput. Phys.*, 174(1) (2001), 381-404.

- [9] D. Ponziani, S. Pirozzoli and F. Grasso, Development of optimized weighted-ENO schemes for multiscale compressible flows, *Int. J. Numer. Meth. Fluids*, 42(9) (2003), 953-977.
- [10] A. K. Henrick, T. D. Aslam and J. M. Powers, Mapped weighted essentially non-oscillatory schemes: Achieving optimal order near critical points, *J. Comput. Phys.*, 207(2) (2005), 542-567.
- [11] E. M. Taylor, M. Wu and M. P. Martín, Optimization of nonlinear error for weighted essentially non-oscillatory methods in direct numerical simulations of compressible turbulence, *J. Comput. Phys.*, 223(1) (2007), 384-397.
- [12] M. Wu and M. P. Martín, Direct numerical simulation of supersonic turbulent boundary layer over a compression ramp, *AIAA J.*, 45(4) (2007), 879-889.
- [13] S. K. Lele, Compact finite-difference schemes with spectral-like resolution, *J. Comput. Phys.*, 103(1) (1992), 16-42.